A&A 528, A21 (2011)
DOI: 10.1051/0004-6361/201016227

Astronomy & Astrophysics

The nearby eclipsing stellar system δ Velorum

II. First reliable orbit for the eclipsing pair⋆,⋆⋆

T. Pribulla[1,2], A. Merand[3], P. Kervella[4], M. Vaňko[2], I. R. Stevens[5], R. Chini[6,7], V. Hoffmeister[6], O. Stahl[8], A. Berndt[1], M. Mugrauer[1], and M. Ammler-von Eiff[9]

[1] Astrophysikalisches Institut und Universitäts-Sternwarte, Schillergäßchen 2-3, 07745 Jena, Germany
e-mail: [alex;markus]@astro.uni-jena.de
[2] Astronomical Institute, Slovak Academy of Sciences, 059 60 Tatranská Lomnica, Slovakia
e-mail: [pribulla;vanko]@ta3.sk
[3] European Southern Observatory, Alonso de Cordova 3107, Vitacura, Santiago, Chile
e-mail: amerand@eso.org
[4] LESIA, Observatoire de Paris, CNRSUMR8109, UPMC, Université Paris Diderot, 5 place Jules Janssen, 92195 Meudon, France
e-mail: Pierre.Kervella@obspm.fr
[5] School of Physics and Astronomy, University of Birmingham, Edgbaston, Birmingham, B15 2TT, UK
e-mail: irs@star.sr.bham.ac.uk
[6] Astronomisches Institut, Ruhr-Universität Bochum, Universitätsstr. 150, 44801 Bochum, Germany
e-mail: [chini;vhoff]@astro.rub.de
[7] Facultad de Ciencias, Universidad Católica del Norte, Antofagasta, Chile
[8] ZAH, Landessternwarte Königstuhl, 69117 Heidelberg, Germany
e-mail: o.stahl@lsw.uni-heidelberg.de
[9] Institut für Astrophysik, Georg-August-Universität, Friedrich-Hund-Platz 1, 37077 Göttingen, Germany
e-mail: ammler@mps.mpg.de

Received 29 November 2010 / Accepted 27 December 2010

ABSTRACT

Context. The nearby multiple system δ Velorum contains a widely detached eclipsing binary and a third component.
Aims. We take advantage of this system offering the opportunity to determine the set of fundamental parameters (masses, luminosities, and radii) of three coeval stars with sufficient precision to test models of stellar evolution.
Methods. Extensive high-resolution spectroscopy is analyzed by the broadening function technique to provide the first spectroscopic orbit of the eclipsing pair. Simultaneous analysis of the spectroscopic data and the SMEI satellite light curve is performed to provide astrophysical parameters for the components. We use a modified Roche model assuming an eccentric orbit and asynchronous rotation.
Results. The observations show that components of the eclipsing pair rotate at about two-thirds of the break-up velocity, which excludes any chemical peculiarity and results in a non-uniform surface brightness. Although the inner orbit is eccentric, no apsidal motion is seen during the SMEI photometric observations. For the inner orbit, the orbital parameters are eccentricity $e = 0.290$, longitude of the periastron passage $\omega = 109°$, and inclination 89.0°.
Conclusions. The component masses of $M_{\rm Aa} = 2.53 \pm 0.11\ M_\odot$, $M_{\rm Ab} = 2.37 \pm 0.10\ M_\odot$, and $M_B \sim 1.5\ M_\odot$ combined with the inferred radii of the Aa and Ab components indicate that the eclipsing pair has already left the main sequence and that the estimated age of the system is about 400 Myr.

Key words. binaries: eclipsing – binaries: spectroscopic – stars: individual: δ Velorum

1. Introduction

δ Velorum is one of the fifty brightest stars in the sky ($V = 1.96$) and is located only 24.4 pc from the Sun ($\pi = 40.90 \pm 0.38$ mas; ESA 1997). For a long time, it has been known that it is a visual binary composed of the brighter component A with $H_P = 1.99$ and the fainter component B with $H_P = 5.57$ orbiting in a wide 142-year orbit (see Argyle et al. 2002).

Surprisingly, observations by visual observers, supported by photometry from the Galileo star tracker, led to the discovery that the brighter component of the visual pair is an eclipsing binary with $P = 45.15$ days (Otero et al. 2000). No complete and reliable observations of both eclipses, however, exist.

Spectroscopic observations of δ Velorum are also very limited. Levato (1972) obtained medium-dispersion (40 Å/mm) photographic spectra of the system and determined an A1V spectral type and a projected rotational speed of $v \sin i = 85\ \mathrm{km\,s^{-1}}$. δ Velorum was later included in the survey of early-type Hipparcos targets of Royer et al. (2002), who took one échelle spectrum of the system. The Fourier transforms of two spectral lines were used to infer that $v \sin i = 150\ \mathrm{km\,s^{-1}}$, which is rather inconsistent with the previous result. These

⋆ Reduced échelle spectra of Delta Velorum are available at the CDS via anonymous ftp to cdsarc.u-strasbg.fr (130.79.128.5) or via
http://cdsarc.u-strasbg.fr/viz-bin/qcat?J/A+A/528/A21
⋆⋆ Table 1 and Figures 5, 6 are only available in electronic form at http://www.aanda.org

measurements very probably included both A and B visual components. No line doubling has been noticed.

The δ Velorum system was observed interferometrically by Kellerer et al. (2007). Their observations consisted of 17 squared visibility measurements using VLTI/VINCI. Although VLTI clearly resolved the eclipsing pair, the presence of the visual component and the small number of observations caused the estimated parameters to be quite uncertain: semi-major axis $a = 5.7\pm0.3\times10^{10}$ m, radii of the components $R_{\rm Aa} = 6.0\pm0.5\,R_\odot$, $R_{\rm Ab} = 3.3\pm0.6\,R_\odot$, eccentricity $e = 0.230\pm0.005$, angle between the major axis and line of sight $\omega' = -(20 \pm 3)^\circ$[1], and longitude of the ascending node $\Omega = 27.4 \pm 1.2^\circ$ with a reduced $\chi^2_r = 2.6$.

Gáspár et al. (2008) discovered a spectacular IR bowshock around δ Velorum at 24 and 70 μm using Spitzer/MIPS images. This very large structure, $\sim1'$, was explained by the authors as a result of the heating and compression of the interstellar medium by the photons from δ Velorum as the trio moves through the interstellar medium. Kervella et al. (2009) resolved the wide visual pair AB using the VISIR and NACO instruments at the VLT and obtained independent photometry of each of the Aa, Ab, and B components. Their photometry did not infer the large radii of the components, found by Kellerer et al. (2007). Mid-infrared observations presented by the authors exclude the presence of a circumstellar thermal excess around the system.

In spite of the above results, it is clear that a robust light-curve (hereafter LC) and spectroscopic analysis are necessary to provide reliable orbital elements and absolute parameters of the components.

2. New observations

2.1. SMEI satellite photometry

Because of its high brightness, δ Velorum is a difficult target for ground-based photometry. Unlike faint stars whose observation quality is dictated mostly by the shot and read-out noise, observations of the brightest stars are affected by the lack of nearby and sufficiently bright comparisons. Accompanying changes/differences in atmosphere transparency result in substantial amount of red noise. Covering eclipses of the eclipsing pair from ground-based observations is complicated by the long orbital period of $P = 45.15$ days.

In the case of δ Velorum, the Solar Mass Ejection Imager (SMEI) provides a LC of sufficient precision. In addition to its primary task, SMEI, attached to the Coriolis satellite, is capable of producing high-precision photometric time-series for stars up to $V = 7$ (see e.g., Bruntt et al. 2006; Tarrant et al. 2008; Spreckley & Stevens, 2008). In a similar way to the MOST satellite (see Walker et al. 2003), Coriolis stays close to the dawn-dusk terminator with an orbital frequency of 14.17 cycles/day. Its three cameras take narrow scans of the sky, but when combined, they provide almost full-sky coverage. Of the 3 cameras that make up SMEI, camera 3 operates at a higher temperature and has degraded photometric performance. We do not use data from camera 3 and this means we do not have continuous coverage of δ Velorum. We refer to Goss et al. (2010) and references therein, for more details about SMEI.

The LC of δ Velorum generated from the SMEI images consist of 11195 points covering 5.6 years. The data were obtained during seven observing seasons (winter half of the year). The photometry is rather sparse, consisting of mostly one observation per the satellite orbit. Owing to the very long orbital period of the eclipsing pair, and the short duration of the eclipses, ΔT (pri) = 0.613 days and ΔT (s) = 0.896 days, only about 350 observations were obtained during the eclipses. By combining nine secondary minima determined from the SMEI photometry and that obtained by the Galileo satellite tracker (Otero, 2000) results in an ephemeris of Min II = HJD 2 447 851.693(9) + 45.15023(7)$\times E$. The SMEI LC does not show apsidal motion. Because of the low angular resolution of the SMEI cameras, both components of the visual pair contribute to the extracted LC.

The quality of the SMEI photometry has been deteriorating since the launch of the satellite. Hence, in the analysis presented here only earlier data (2003–2006) have been used (Fig. 1).

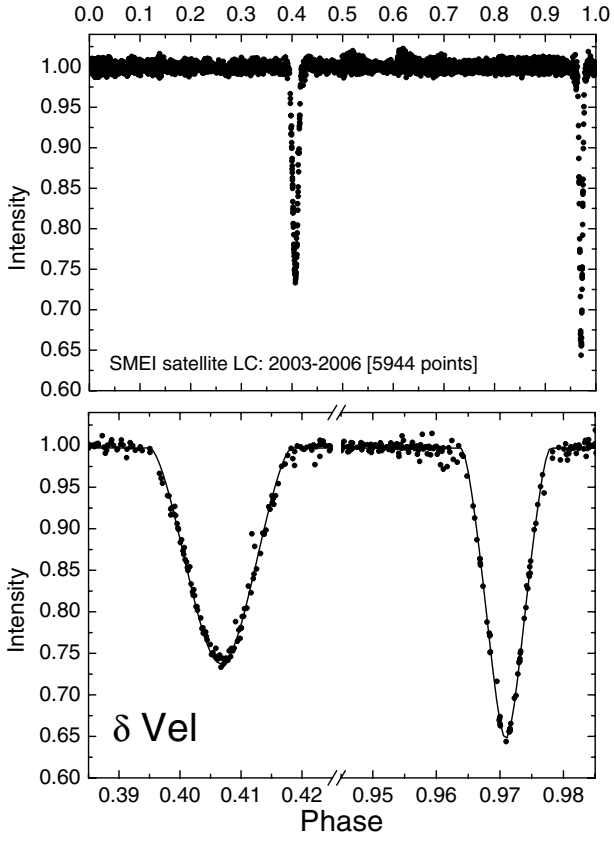

Fig. 1. Detrended and filtered (removing obvious outliers) SMEI LC of δ Vel. The data were phased using the following ephemeris for the periastron passage: To = HJD 2 452 528.950 + 45.15023$\times E$ (see Table 2). Only data from 2003-2006 are plotted.

2.2. BESO spectroscopy

Available spectroscopy of δ Velorum is very limited in spite of its brightness of $V = 1.96$. Two high-resolution échelle spectra are available in the ESO/FEROS data archive taken on November 25, 2004 and January 7, 2009 (both outside eclipses). There is practically no difference in the shape of the line profiles between the two spectra nor any indication that δ Velorum is a SB2 system. The system has also been observed by ESO/HARPS. Unfortunately, the spectra available in the ESO archive do not sufficiently cover the orbital cycle and are of low signal-to-noise ratio (S/N).

New optical spectroscopy of δ Velorum has been obtained at the Cerro Armazones Observatory using the BESO échelle spectrograph fiber-fed from the Cassegrain focus of the 1.5 m Hexapod Telescope (hereafter HPT, see Fuhrmann et al. 2010).

[1] This angle transforms into a longitude of periastron of $\omega = 90^\circ - \omega'$.

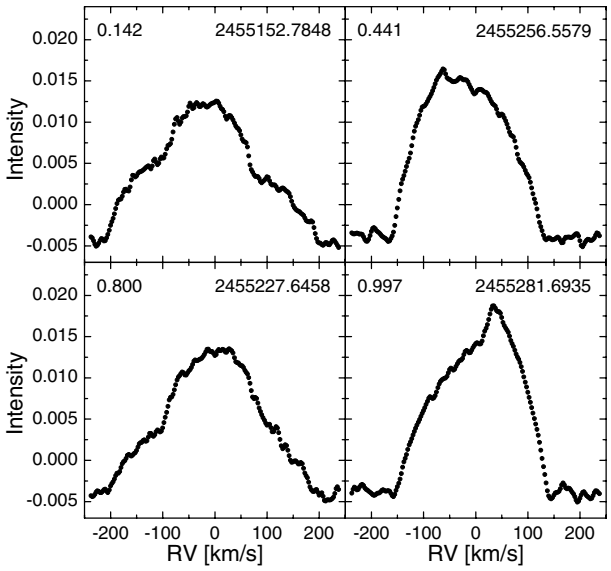

Fig. 2. Broadening functions close to the principal phases (counted from the primary eclipse, with the secondary occurring at phase 0.436): 0.142 (maximum separation of the components), 0.441 (end of the secondary eclipse), 0.800 (maximum separation of the components), and 0.997 (beginning of the primary eclipse). The radial velocity system is barycentric. Full mosaic showing all BFs including best fits is shown in Fig. 6.

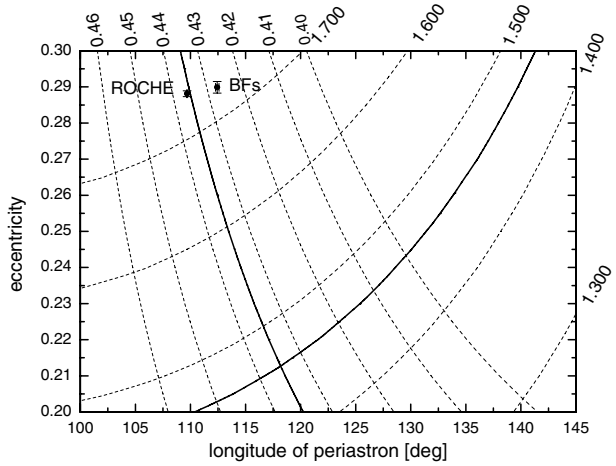

Fig. 3. Phase of the secondary minimum (labelled values are 0.40–0.46; the observed phase is 0.436) and ratio of minima durations (with labelled values 1.3–1.7; the observed ratio is 1.462). The lines are valid for an inclination angle of ~90°. Thick solid lines represent the observed values and their intersection indicates that $e = 0.20$–0.22 and $\omega = 115$–$120°$. The resulting orientation and eccentricity of the orbit plotted for simple BF modelling (Sect. 3.2) and ROCHE modelling (Sect. 3.3) shows that $i < 90°$.

Sixty-three spectra were obtained between April 2009 and April 2010. The spectra cover a 3530–8860 Å wavelength range. The data were reduced using dedicated ESO-MIDAS scripts. The photometric reduction includes overscan, bias, and flat-field correction. In subsequent steps individual échelle orders were then extracted, wavelength calibrated, and normalized to the continuum. Finally, cosmic-ray spikes were removed. Wavelength calibration was later improved using telluric bands close to 6900 and 7600 Å using the spectrum of η CMa as the telluric template. The improved RV system is stable to about 100 m s^{-1} as indicated by the RV difference between the spectral bands mentioned above. The absolute zero point of the system has not, however, been checked. Therefore, the systemic velocity of δ Velorum may be offset from its true value.

According to the VLT/NACO imaging of Kervella et al. (2009), the separation of the optical pair A-B was about 0.6″ in 2008. Because of a PSF of 3–5″ at the HPT, both visual components were included in the fiber entrance. Hence, it is reasonable to assume that no light from the faint companion has got lost. The PSF required exposure times of typically 300–900 s, resulting in S/N ratios ranging from about 100 to 400. The journal of observations can be found in Table 1.

The aforementioned sixty-three spectra cover more-or-less uniformly the orbital cycle of δ Velorum. Several spectra were intentionally taken during the eclipses. All reduced one-dimensional spectra will be available at the CDS.

3. Data analysis

3.1. Orientation of the orbit

In principle, the orientation and eccentricity of the orbit can be estimated from the position (phase) of the secondary minimum and ratio of the minima durations (see analysis of Kellerer et al. 2007). If we denote the deeper minimum as the primary and assume that the orbit is seen edge-on, from the observed minima durations and secondary minimum phase in the case of δ Velorum, one infers that $e = 0.20$–0.22 and $\omega = 115$–$120°$ (see Fig. 3). The longitude of the periastron refers to the orbit of the *component eclipsed in the primary minimum*. When we refer to the orbit of the component eclipsed in the secondary minimum, we must convert $\omega \rightarrow \omega + 180°$.

The case of eccentric orbits with $i \neq 90°$ is not that simple because (i) the ratio of minima depths does not reflect the ratio of the surface brightnesses of the components (in the deeper, primary minimum even the *cooler* and *less massive* component can be eclipsed); (ii) the ratio of minima width cannot be used to find $e \sin \omega$. If $\omega \neq 90°$ nor 270°, for sufficiently low inclination angles the minimum occurring further away from the periastron can disappear and the observer can detect only one system of minima. This is the case for e.g., BD+37 410 (Pribulla et al. 2010) or NY Cep (see Holmgren et al. 1990).

None of the minima of δ Velorum (see Fig. 1) shows a constant brightness interval. This means that at least one minimum is partial[2] with $i < 90°$. Hence, exact eclipse modeling is needed to derive reliable parameters.

3.2. Extracting Doppler information and a preliminary orbit

Besides the Balmer series, there are few other strong lines in the optical spectrum of δ Velorum. The optimal spectral region for extracting Doppler information is the blue spectrum between 4370–4605 Å. In addition to the fairly strong Mg II 4481, line it contains many weaker metallic lines (mostly of Fe I) but is devoid of hydrogen lines. This blue part of the spectra was deconvolved using a high-resolution synthetic spectrum corresponding to $T^{\rm eff} = 9500$ K, $\log g = 4.5$, solar metallicity[3], and, a non-rotating star to obtain broadening functions (BFs) using the formalism developed by Rucinski (1992). Extracted

[2] Total minimum can still be a transit, curved because of the limb darkening.

[3] The spectrum was taken from the Pollux database available online at http://pollux.graal.univ-montp2.fr/

BFs were smoothed by convolving with a Gaussian function ($\sigma = 10$ km s^{-1}) to match the spectral resolution of BESO.

The template provided a very good match to the observed spectra indicated by the BF integral being close to unity (on average about 0.97). Using a hotter template with $T^{\rm eff} = 10\,000$ K, $\log g = 4.5$, and metallicity 0.5 dex lower than the solar one, we derived BF integrals of about 1.58. The BF integral depends on the strength of metallic lines in the region, hence a good spectral match can be provided by synthetic template of lower temperature and lower metallicity or by using a template of higher temperature and higher metallicity.

Extracted BFs clearly show that δ Velorum is a SB2. Unfortunately, profiles of the components are always blended (see Fig. 2). The orbital motion can be, however, well seen from strong changes in the total width and shapes of BFs. The deformed shapes of BFs close to spectroscopic conjunctions confirm that eclipses are detected in the system. We note that the extracted BFs do not show any presence of the visual component B in the system despite its expected contribution of about 3.7% (in the wide H_p passband[4]). We also produced an average spectrum of δ Velorum and extracted the corresponding BF. In this way, the orbital motion of the eclipsing pair is smeared-out but no additional component can be seen. This indicates that the visual component B is also a rapid rotator or a SB1/SB2 system. Another possible explanation is that the spectral type of the third component is too different to be picked up in the spectrum using the A0 template.

Because the profiles of the components are never separated and we observe only blends of variable shape, it is impossible to directly determine the RVs of the components. Hence, we modeled the whole dataset (with a single set of parameters) assuming that (i) the width and shape of the rotational profiles of the components do not change with phase; (ii) the relative intensity of the components is constant; (iii) the limb darkening is the same for both components; (iv) there is no apsidal motion visible in our data (as indicated by the long-period of the eclipsing pair); and (v) stars rotate as solid bodies (no differential rotation). To fulfill the first two conditions, the spectra taken during the eclipses were neglected. The standard deviation of each BF was determined using its violet part which was always outside of the component's profiles.

In the case of solid-body rotation and a linear limb-darkening law, the rotational profile is an analytic function. The BF observed outside the eclipses is just the sum of two rotational profiles as given by Gray (1976). The limb darkening coefficient was fixed to be $u_{\rm Aa} = u_{\rm Ab} = 0.522$ as appropriate for an A0V star ($T^{\rm eff}_{\rm A} = 9420$ K, Popper, 1980) with $\log g = 4.5$ and $\lambda = 4400$ Å. Global fitting to all observed BFs included the following parameters: orbital eccentricity e; longitude and time of the periastron passage T_0, ω; systemic velocity V_A; sum of semi-amplitudes of the RV changes $K_{\rm Aa}+K_{\rm Ab}$; mass ratio $q = M_{\rm Ab}/M_{\rm Aa}$; background level of BFs[5] B_0; intensities of the profiles $I_{\rm Aa}$, $I_{\rm Ab}$; and projected rotational velocities of the components $v_{\rm Aa} \sin i$, $v_{\rm Ab} \sin i$. The orbital period P was held fixed at the photometrically determined value, $P = 45.15023$ days, because of the relatively short timespan of the observations.

[4] The maximum response of the Hipparcos photometric system lies within spectral range used to extract the BFs.

[5] For both a perfect match between the spectral types of the template and observed star and proper rectification to the continuum, it should be zero.

Table 2. Parameters of the eclipsing pair in the δ Velorum system.

		BF fitting	ROCHE
Assumed parameters			
P	[days]	45.15023(7)	45.15023(7)
$\beta_{\rm Aa} = \beta_{\rm Ab}$		–	0.25
$A_{\rm Aa} = A_{\rm Ab}$		–	1.00
π	[mas]	–	40.90(38)
$L_3 = l_{\rm B}/(l_{\rm Aa} + l_{\rm Ab})$		–	0.048
$T^{\rm eff}_{\rm Aa}$	[K]	–	9420
Optimized parameters			
T_0	[HJD]	529.185(11)	528.950(5)
e		0.2899(16)	0.2881(8)
i	[deg]	–	89.00(3)
ω	[deg]	112.43(16)	109.69(5)
$\Omega_{\rm Aa}$		–	34.3(4)
$\Omega_{\rm Ab}$		–	35.7(4)
$F_{\rm Aa}$		–	43.2(7)
$F_{\rm Ab}$		–	50.3(9)
$q = M_{\rm Ab}/M_{\rm Aa}$		0.938(11)	0.937(10)
$K_{\rm Aa} + K_{\rm Ab}$	[km s^{-1}]	104.8(2)	106.0(15)
V_A	[km s^{-1}]	−12.07(5)	−10.4(5)
$v \sin i_{\rm Aa}$	[km s^{-1}]	139.48(10)	139.4
$v \sin i_{\rm Ab}$	[km s^{-1}]	146.84(13)	146.5
χ^2_r (LC)		–	0.852
χ^2_r (BF)		2.710	1.945
Computed parameters			
$A \sin i$	[$R_\odot$]	89.5(2)	90.6(9)
$M_{\rm Aa} \sin^3 i$	[$M_\odot$]	2.44(2)	2.53(11)
$M_{\rm Ab} \sin^3 i$	[$M_\odot$]	2.29(2)	2.37(10)
$L_{\rm Aa}$	[$L_\odot$]	–	56.3(17)
$L_{\rm Ab}$	[$L_\odot$]	–	47.1(25)
$l_{\rm Ab}/l_{\rm Aa}$		0.813(3)	0.822(4)
$R_{\rm Aa}$	[$R_\odot$]	–	2.83(4)
$R_{\rm Ab}$	[$R_\odot$]	–	2.54(5)
$\log g_{\rm Aa}$	[cgs]	–	3.90(2)
$\log g_{\rm Ab}$	[cgs]	–	3.97(3)

Notes. In both cases (rotational profile fitting to BFs, Sect. 3.2, and full ROCHE modelling, Sect. 3.3), the orbital period, P, corresponds to the best linear fit to the Galileo and SMEI secondary minima (see Sect. 2.1). Third light L_3 has been estimated for the SMEI passband using model atmospheres. Heliocentric Julian date of the periastron passage is −2 452 000. Reduced χ^2_r is separately given for LCs and BFs. Generalized equipotentials are given for the mean distance (not in the periastron passage). Projected rotational velocities in the case of the combined ROCHE solution were not optimized but computed from other parameters. The ratio of fluxes, $l_{\rm Ab}/l_{\rm Aa}$, is given in the SMEI passband.

The convergence process was repeated starting at many (dozens) parameter sets. Modeling showed that the component eclipsed in the primary minimum is the more massive of the two.

The optimization always resulted in the same parameters (listed in Table 2) indicating uniqueness of the solution (see Fig. 5 showing fits to all BFs outside eclipses). The effect of the limb darkening is small but not negligible. For the acceptable temperature range, 8750 K (A2V) to 10 000 K (B9.5V), the principal parameters lie within the following ranges: e = [0.2889, 0.2924], $K_{\rm Aa} + K_{\rm Ab}$ = [104.41, 105.27] km s^{-1}, $v_{\rm Aa} \sin i$ = [139.11, 140.21] km s^{-1}, and $v_{\rm Ab} \sin i$ = [146.48, 147.58] km s^{-1}. It is clear that the systematic uncertainties (connected with the uncertain temperature and the limb darkening coefficient) are larger than those determined from residuals and the covariance matrix. The reduced χ^2_r corresponding to the tested temperature range changes by only 3.1% (lowest χ^2_r occurs for $T^{\rm eff}$ = 8750 K). For any solution, it is clear that the component being

eclipsed in the primary minimum is the more massive of the two. The goodness of the fit, $\chi^2_r = 2.71$ is indicative of underestimated errors in the BFs or/and a too simple model being used to fit the data.

For the solution corresponding to A0V stars, the ratio of fluxes is

$$\frac{l_{\rm Ab}}{l_{\rm Aa}} = \frac{I_{\rm Ab} v_{\rm Ab} \sin i}{I_{\rm Aa} v_{\rm Aa} \sin i} = 0.813(3). \quad (1)$$

The brightness ratio should be interpreted with caution because in extracting BFs the same template was used for both components. In the case that the spectral type of the secondary was later (or better strength of the metallic lines was larger) the estimated light ratio is the upper estimate. Results of the following Sect. 3.3 indicate, however, that the temperatures of the components are very similar.

The corresponding masses of the components are $M_{\rm Aa} \sin^3 i = 2.439(20)\ M_\odot$, and $M_{\rm Ab} \sin^3 i = 2.288(18)\ M_\odot$ (the mass ratio is then 0.938(11)). Considering the full acceptable range of temperatures, the masses fall within $2.4308 < M_{\rm Aa} \sin^3 i < 2.4516\ M_\odot$ and $2.2709 < M_{\rm Ab} \sin^3 i < 2.2950\ M_\odot$. Because the inclination angle is ~89° (see Sect. 3.3), the projected masses are close to the true masses (a 1% increase in mass occurs for an inclination $i = 85.3°$).

The BFs, very probably, contain a weak signature of the visual component B. Its separate spectrum would, however, be needed to remove its influence on BFs and the determined orbital elements. If it were a single but rapidly-rotating star (having a profile with a constant RV), it would effectively bring the components of the eclipsing pair together, reducing ($K_{\rm Aa} + K_{\rm Ab}$) and also alter the derived rotational velocities. Because of a severe blending of the primary and secondary lines, it is also impossible to check whether the components rotate as a solid body or differentially.

3.3. Simultaneous analysis of photometry and spectroscopy

Assuming that the apsidal motion is very slow[6] and the orbital period is stable, we can combine SMEI (broadband) LC and OCA échelle spectroscopy (63 BFs) to help us derive consistent parameters for the system.

Data modeling has been performed using an updated version of the code *ROCHE* (Pribulla, 2004). The code assumes Roche model defining the surface geometry and local gravity on the components. Solid-body rotation was assumed. It is assumed (as suggested by Wilson, 1979) that the components can adjust their shape[7] to slightly changing equipotential surfaces in the case of an eccentric orbit. The generalization of the Roche model for asynchronous rotation was also applied. Surface grids are derived from an icosahedron, resulting in practically equal elements. For both stars, it was assumed that the Von Zeipel (1924) law (appropriate for radiative envelopes) dictates local temperature. Single mutual reflection/irradiation was computed.

The optimized parameters are as follows: inclination angle i, generalized equipotentials $\Omega_{\rm Aa}$, $\Omega_{\rm Ab}$, asynchronous rotation factors $F_{\rm Aa}$, $F_{\rm Ab}$[8], mass ratio q, polar temperature of the secondary $T^{\rm eff}_{\rm Ab}$, sum of semi-amplitudes $K_{\rm Aa} + K_{\rm Ab}$, systemic velocity $V_{\rm A}$, longitude of periastron ω, eccentricity e, global normalization factor of BFs (should be unity in the case of perfect template match), and the global level of the BF background. Linear limb darkening coefficients $u_{\rm Aa}$, $u_{\rm Ab}$ were automatically recalculated, interpolating from tables of van Hamme (1993) according to the mean surface gravity and wavelength range (separately for LCs and BFs). Local surface intensities were interpolated from tables of Lejeune et al. (1997) for each surface grid point. Because of the changing distance and shape of the components, both the surface grid and local parameters had to be recalculated for each step in phase (360 steps/orbit). During the eclipses, a four-times finer phase step was used.

The scatter in *whole* individual datasets was estimated by performing polynomial fitting to constant regions: in the case of the SMEI LC, we used out-of-eclipse phases, for BF parts outside the blended profile. To constrain the solution more tightly, only eclipse parts of the SMEI LC were used. Resulting parameters are listed in Table 2. The combined solution gives true (not projected) masses of the components as $M_{\rm Aa} = 2.53 \pm 0.11\ M_\odot$ and $M_{\rm Ab} = 2.37 \pm 0.10\ M_\odot$ ($\sin^3 i = 0.99954$).

The best fits to both eclipses, as observed by the SMEI satellite, are shown in Fig. 1, and fits to all BFs are available in Fig. 6. The best fits to the BFs including eclipses do not uncover any systematic discrepancies. Small differences in the shapes of the minima branches of the SMEI LC can, however, be seen. This may be the result of a simplified treatment of the limb darkening effect[9] or small departures of the component shapes from the generalized Roche model. By comparing spectroscopic elements obtained by assuming two limb-darkened rapidly rotating spheres (Sect. 3.2) to those obtained by the more realistic modeling by assuming a Roche geometry including all proximity effects, we find that the results are quite reliable. The major difference between the two cases concerns the mass ratio and the total mass of the system (given by $K_{\rm Aa} + K_{\rm Ab}$), which is higher in the case of full modeling.

Because of the enormous amount of CPU time required to model the deformed (and varying) shapes of the components with the orbital revolution, it is practically impossible to survey the whole parameter space and any possible correlations between parameters. Some properties of the solution and of information contained in the data are as follows:

- unlike LCs, the BFs alone do not define both the eccentricity and the orientation of the orbit very well. Fixing eccentricity at different reasonable values gives acceptable range $e = [0.24, 0.33]$ without any obvious correlation to ω, always being $[112, 116]°$;
- the LC alone defines inclination angle very well because of the small fractional radii of the components, but there is a correlation between the radii of the components and the inclination angle. The solution shows that *both* eclipses are partial – the visible surfaces of the component eclipsed in the minima are 35.6% (primary minimum) and 40.8% (secondary minimum);
- including asynchronous rotation in the computation of the component's shapes does not improve the solution significantly. The presence of fast asynchronous rotation cannot be inferred from the photometry alone. The information content

[6] Using formulae of Hilditch (1980), resulting parameters from Table 2 and corresponding apsidal constants adopted from Claret (2004) for 400 Myr stellar model with overshooting (see Sect. 4) leads to $U \sim 6$ Myr.

[7] In the case of δ Velorum, an eccentric orbit causes very small changes in the true radii with orbital phase, e.g., $\Delta R_{\rm point}/R \sim 7 \times 10^{-5}$. The shapes of the components are much more affected by fast asynchronous rotation.

[8] For bound rotation, $F_{\rm Aa} = F_{\rm Ab} = 1$.

[9] The limb-darkening coefficients are assumed to be constant over the surface of components.

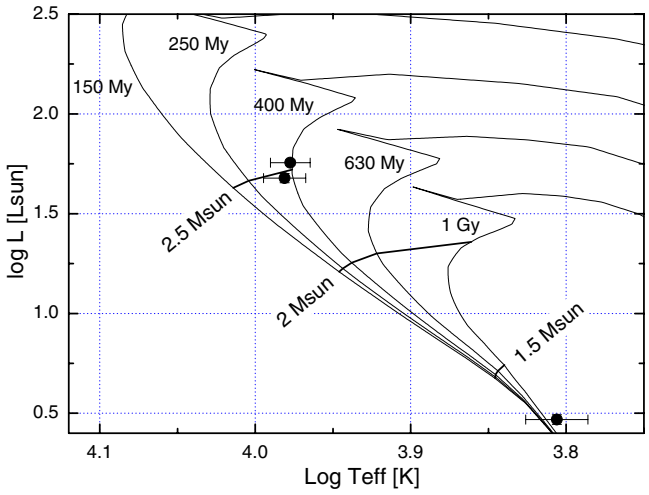

Fig. 4. Theoretical isochrones for solar composition ($X = 0.70$, $Y = 0.28$, $Z = 0.02$) assuming overshooting adopted from Claret (2004). Positions of all three components of δ Velorum are shown. Thick solid lines correspond to masses 1.5 $M_\odot$, 2 $M_\odot$, and 2.5 $M_\odot$. Luminosities of Aa and Ab correspond to the combined solution, while for component B the luminosity was derived from the Hipparcos distance and observed visual magnitude. Horizontal error bars for the components of the eclipsing pair correspond to the surface temperature ranges due to the gravity brightening.

of one broad-band LC is clearly much smaller than that of many BFs obtained at different phases.

- by assuming no gravity darkening ($\beta_{\rm Aa} = \beta_{\rm Ab} = 0.00$), the fits to the LCs and BFs become poorer by only 5% and 2% (according to χ^2_r). This means that it is impossible to reliably determine the gravity darkening coefficient from the present data;
- the combined solution shows that the secondary component is slightly hotter than the primary. This information cannot be inferred from BF modeling alone.

4. The triple system δ Velorum

The total mass of the whole triple system δ Velorum as determined by Argyle et al. (2002) is rather uncertain: $5.71^{+1.27}_{-1.08}$ $M_\odot$ (assuming the Hipparcos parallax, $\pi = 40.90 \pm 0.38$ mas). The authors give visual magnitudes of the components as $V_A = 1.97$ and $V_B = 5.55$, corresponding to absolute magnitudes of $M_V(A) = 0.02$ and $M_V(B) = 3.60$. The visual orbit was determined based on the data from 1895 until 1999. Because of the most recent periastron passage (2000.8 according to their orbit), any new positional measurements of the visual pair could significantly improve the orbit. The new observation (NACO/VLT on April 1, 2008) of Kervella et al. (2009) enables us to measure a separation between the components of about 0.6″ (their Fig. 2), confirming the orbit of Argyle et al. (2002).

Our combined LC and BF solution gives the following luminosities for the components: $L_{\rm Aa} = 56.3$ $L_\odot$ and $L_{\rm Ab} = 47.1$ $L_\odot$. Taking the absolute bolometric magnitude of Sun as $M^{\rm bol}_\odot = 4.75$ and bolometric correction for components of δ Vel (A0V) as B.C. = −0.15 (Popper 1980), we derive the absolute visual magnitudes of the components to be $M_V(Aa) = +0.519$ and $M_V(Ab) = +0.719$. This gives a combined magnitude of $M_V(A) = -0.138$, which is substantially brighter than the reliable value determined from the observed visual brightness and Hipparcos distance by Argyle et al. (2002). This simple computation, however, does not take into account that the observer faces the coldest (equatorial) part of the system. The apparent magnitudes of the eclipsing pair synthesized by the *ROCHE* code (including all proximity effects and gravity darkening), $U = 1.98 \pm 0.02$, $B = 1.94 \pm 0.02$, $V = 1.95 \pm 0.02$, and $K = 1.86 \pm 0.02$ are in very good agreement with the observations: Kervella et al. (2009) found V (Aab) = 2.00 ± 0.02 and K (Aab) = 1.86±0.09.

The positions of all three components in the H-R diagram and the theoretical isochrones are plotted in Fig. 4. Assuming that the third component is still on the main sequence[10], its absolute visual magnitude, $M_V(B) = 3.60$, corresponds to F2-F5 spectral type or according to Cox (2000) to $T^{\rm eff}_{\rm B} = 6100$–$6700$ K and luminosity $L_{\rm B} = 3.19$–3.56 $L_\odot$. In the H-R diagram, component B is slightly above the main sequence, supporting the earlier limit for the spectral type, namely F2V. The positions of components of the eclipsing pair Aa, Ab plotted in Fig. 4 were derived from the combined solution to all BFs and SMEI LC for $T^{\rm eff}_{\rm Aa} = 9420$ K.

The observed masses and radii of the components correspond most closely to the model predictions (Claret 2004, $Y = 0.70$, $Z = 0.02$, and overshooting) for 400 Myr, when the temperatures of components are assumed to be $T_{\rm Aa} = 9470$ K, $T_{\rm Ab} = 9370$ K, $R_{\rm Aa} = 2.643$ $R_\odot$, and $R_{\rm Ab} = 2.363$ $R_\odot$. The corresponding apsidal motion constants are $\log k_2$ (Aa) = −2.4972 and $\log k_2$ (Ab) = −2.4626. The observed radii of stars are still about 5–6% larger, giving additional support to measurements of lower temperature and a slightly older age than 400 Myr – soon after 400 Myr, the temperatures of the components equalize (as observed) because of the slightly faster evolution of the more massive primary component. The next isochrone available from Claret (2004) for 630 Myr predicts that $T_{\rm Aa} = 7980$ K, $T_{\rm Ab} = 8132$ K, $R_{\rm Aa} = 4.263$ $R_\odot$, and $R_{\rm Ab} = 3.393$ $R_\odot$. The evolution of the components could, however, be affected by fast rotation, making the main-sequence phase last longer (see e.g., de Mink 2010).

5. Discussion and future work

Our new data has enabled the first sound analysis of the eclipsing pair Aab in the δ Velorum system. The main results are as follows:

- both minima are partial. For the given orientation of the orbit and assuming (fairly similar) the derived radii of components, the total eclipse and annular transit occur only if $i > 89.8°$;
- the components of the eclipsing pair are a factor of two smaller than derived interferometrically by Kellerer et al. (2007);
- the brightness ratio of brightness of components in the SMEI passband (close to the R passband) is about 0.823. The components are of similar temperature, however, both very probably being of spectral type A1V. This is strongly supported by a close agreement with the synthetic depth of the primary minimum in the K passband Δmag $I = 0.430$, while Kervella et al. (2009) determined Δmag $I = 0.440 \pm 0.011$ from the NACO imaging during the primary eclipse;
- there is no apsidal motion in the system observed during the six-year time-series of the SMEI data as indicated by the observed times of the minima;

[10] It is the least massive of the trio, with a significant turn-off from the main sequence at ages older than 1 Gyr, excluded by the evolutionary state of the eclipsing pair.

- photocenter motion of the eclipsing pair (corresponding to our solution) is only about 1 mas: it was not detected by the Hipparcos satellite;
- both components rotate very rapidly: the primary at about 56% of the break-up velocity, the secondary at about 62%. This also means that the components are strongly deformed. When the surface can be accurately described by a generalized ROCHE model, the polar flattening of the components is 1/10 and 1/12. Because of the fast rotation, the surface temperatures are rather non-uniform. The von Zeipel theorem predicts the following ranges: 9220 K $< T_{\rm Aa}^{\rm eff} <$ 9780 K and 9280 K $< T_{\rm Ab}^{\rm eff} <$ 9880 K[11]. This effect should be confirmed by long-baseline interferometry;
- the best fits to the BFs extracted during the primary transit (spectra taken at phases 0.995, 0.997, 0.000, and 0.002) shows just slight deviations indicating that the rotational axis of the primary component is almost perpendicular to the orbital plane. The secondary minimum, occurring around phase 0.436, is insufficiently covered (a single spectrum at phase 0.441) by the spectroscopic observations to be able to derive any information about the rotational axis orientation;
- the spectral type of δ Velorum A is most probably A1V, although different approaches infer a fairly wide range of results: (i) the BF strength indicates that $T_A^{\rm eff} = 9500$ K (A0V) (see Sect. 3.2); (ii) a combination of the observed visual brightness, Hipparcos distance, and radii of the components (simultaneous solution in Sect. 3.3) supports a similar temperature, 9420 K; (iii) the observed colors $U-V = 0.11$, $B-V = 0.04$, $V-R = 0.05$, and $V-I = 0.09$ imply a later classification, A1-2V (see Stickland & Hucht, 1977); (iv) the shape and intensity of the H_β line (in our BESO spectra) corresponds most closely to a higher temperature, $T_{\rm A}^{\rm eff} =$ 10 000 K and $\log g_{\rm A} = 4.5$–4.6 (B9.5V); and (v) Gray (2006) gives a spectral type of A1Va(n), $T^{\rm eff} = 9021$ K, $\log g = 3.79$, and $\log$ [M/H] $= -0.33$. Because the system is very close, no interstellar reddening is expected. On the other hand, the presence of circumstellar material around δ Velorum cannot be fully excluded.

In spite of significant progress, the astrophysical parameters of δ Vel should still be verified. The total mass of the system is slightly affected by the unknown nature (multiplicity, rotation rate) of the third component (δ Velorum B). To correctly remove its contribution to the observed line profiles, it will be necessary to acquire its spectrum separately. This task will not be easy: the separation between the components will become smaller until 2013 when it reaches 0.38″. The separation then should slowly increase until 2067, reaching about 2.9″.

Our phase-resolved spectra may still need to be precessed by the Fourier disentangling (see Hadrava, 1995) to obtain the individual spectra of components and their astrophysical parameters ($\log g$, $T^{\rm eff}$, metallicity etc.). Because of the strong rotational mixing, any chemical peculiarity is, however, excluded. Most importantly, the combination of the present data with long-baseline interferometry will be required, which may possibly detect the flattening of the components and "polar caps" brightening caused by the rapid rotation. This additional dataset would break the parameter correlations complicating the present modeling.

Additional high-resolution spectroscopy should be secured during the eclipses to study the Rossiter-McLaughlin effect. Photometric eclipse modeling can still be improved by dedicated multi-color photometry of the transits, which is important for a clearer definition of the surface brightness ratio.

Another possible way to improve the outer visual orbit is to use timing of the minima of the eclipsing pair, which should show a light-time effect. The expected semi-amplitude, for the visual orbit of Argyle et al. (2002), is about 1.5 h. In view of the large $v \sin i$ of the components and the blending of their profiles, systemic-velocity changes in the eclipsing pair would be hardly detectable nor useful.

Acknowledgements. M.V. and T.P. acknowledge support from the EU in the FP6 MC ToK project MTKD-CT-2006-042514. This work has partially been supported by VEGA project 2/0038/10.

This publication is supported as a project of the Nordrhein-Westfälische Akademie der Wissenschaften und der Künste in the framework of the academy program by the Federal Republic of Germany and the state Nordrhein-Westfalen.

M.A. acknowledges research funding granted by the *Deutsche Forschungsgemeinschaft* (DFG) under the project RE 1664/4-1. A.B. acknowledges support from DFG in program NE 515/32-1.

The research made use of the SIMBAD database, operated at the CDS, Strasbourg, France.

References

Argyle, R. W., Alzner, A., & Horch, E. P. 2002, A&A, 384, 171
Bruntt, H., Southworth, J., Torres, G., et al. 2006, A&A, 456, 651
Claret, A. 2004, A&A, 424, 919
Cox, C. W. 2000, Allens Astrophysical Quantities (Springer Verlag)
de Mink, S. 2010, Ph.D. Thesis, Utrecht University
European Space Agency 1997, The Hipparcos and Tycho Catalogues (ESA SP-1200) (Noordwijk: ESA)
Fuhrmann, K., Chini, R., Hoffmeister, V. H., et al. 2010, MNRAS, in press
Gáspár, A., Su, K. Y. L., Rieke, G. H., et al. 2008, ApJ, 672, 974
Goss, K. J. F., Karoff, C., Chaplin, W. J., Elsworth, Y., & Stevens, I. R. 2010, MNRAS, in press
Gray, F. D. 1976, The Observation and Analysis of Stellar Photospheres (New York: Wiley)
Gray, R. O., Corbally, C. J., Garrison, R. F., et al. 2006, AJ, 132, 161
Hadrava, P. 1995, A&AS, 114, 393
Hilditch, R. W. 2001, An Introduction to Close Binary Stars, (Cambridge: University Press), 140
Holmgren, D. E., Hill, G., Fisher, W., & Scarfe, C. D. 1990, A&A, 231, 89
Kellerer, A., Petr-Gotzens, M. G., Kervella, P., & Coudé du Foresto, V. 2007, A&A, 469, 633
Kervella, P., Thévenin, F., & Petr-Gotzens, M. G. 2009, A&A 493, 107
Lejeune, Th., Cuisinier, F., & Buser, R. 1997, A&AS 125, 229
Levato, O. H. 1972, PASP, 84, 584
Otero, S. A., Fieseler, P. D., & Lloyd, C. 2000, IBVS No. 4999
Popper, D. M. 1980, ARA&A, 18, 115
Pribulla, T. 2004, in Spectroscopically and Spatially Resolving the Components of the Close Binary Stars, ed. R. W. Hilditch, H. Hensberge, & K. Pavlovski, ASP Conf. Ser., 318, 117
Pribulla, T., Rucinski, S. M., Latham, D. W., et al. 2010, AN, 331, 397
Royer, F., Gerbaldi, M., Faraggiana, R., & Gómez, A. E. 2002, A&A, 381, 105
Rucinski, S. M. 1992, AJ, 104, 1968
Spreckley, S. A., & Stevens, I. R. 2008, MNRAS, 388, 1239
Stickland, D. J., & van der Hucht, K. A. 1977, A&A, 54, 883
Tarrant, N. J., Chaplin, W. J., Elsworth, Y. P., Spreckley, S. A., & Stevens, I. R. 2008, A&A, 492, 167
van Hamme, W. 1993, AJ, 106, 2096
von Zeipel, H. 1924, MNRAS, 84, 665
Walker, G., Matthews, J., Kuschnig, R., et al. 2003, PASP, 115, 1023
Wilson, R. E. 1979, ApJ, 234, 1054

Pages 8 to 15 are available in the electronic edition of the journal at http://www.aanda.org

[11] Surface temperature increases from the equator to the poles.

Table 1. Journal of spectroscopic observations at Cerro Armazones Observatory.

Spectrum	BJD 2 400 000+	Phase	S/N	Exp. [s]	Spectrum	BJD 2 400 000+	Phase	S/N	Exp. [s]
20090429-01.fits	54 951.47364	0.6839	193	600	20100117-11.fits	55 214.72408	0.5145	233	600
20091019-21.fits	55 124.88346	0.5247	195	300	20100120-06.fits	55 217.68788	0.5801	175	600
20091019-22.fits	55 124.88728	0.5248	193	300	20100121-04.fits	55 218.66777	0.6018	259	600
20091019-23.fits	55 124.89110	0.5248	198	300	20100122-05.fits	55 219.66618	0.6239	232	600
20091020-20.fits	55 125.89151	0.5470	190	300	20100123-06.fits	55 220.62644	0.6452	223	600
20091020-21.fits	55 125.89535	0.5471	196	300	20100125-05.fits	55 222.68527	0.6908	207	600
20091021-18.fits	55 126.89139	0.5691	203	300	20100127-04.fits	55 224.66181	0.7346	204	600
20091022-25.fits	55 127.87589	0.5909	207	300	20100128-02.fits	55 225.67460	0.7570	229	600
20091022-26.fits	55 127.88004	0.5910	203	300	20100130-02.fits	55 227.64583	0.8007	176	600
20091022-27.fits	55 127.88384	0.5911	215	300	20100131-02.fits	55 228.70596	0.8242	168	600
20091023-18.fits	55 128.88626	0.6133	218	300	20100208-01.fits	55 236.65951	0.0003	113	600
20091023-19.fits	55 128.89015	0.6134	193	300	20100208-06.fits	55 236.76622	0.0027	121	600
20091024-20.fits	55 129.88268	0.6354	188	300	20100211-04.fits	55 239.66155	0.0668	272	600
20091112-15.fits	55 148.81797	0.0548	212	300	20100214-10.fits	55 242.71579	0.1345	210	600
20091112-16.fits	55 148.82182	0.0549	234	300	20100217-09.fits	55 245.66592	0.1998	241	600
20091116-05.fits	55 152.78108	0.1426	247	300	20100220-07.fits	55 248.58518	0.2644	202	600
20091116-06.fits	55 152.78487	0.1426	261	300	20100226-08.fits	55 254.68385	0.3995	383	1800
20091116-09.fits	55 152.85198	0.1441	221	300	20100228-04.fits	55 256.55795	0.4410	262	600
20091118-04.fits	55 154.76307	0.1865	213	300	20100228-13.fits	55 256.72306	0.4447	281	600
20091118-05.fits	55 154.76687	0.1865	224	300	20100304-07.fits	55 260.66669	0.5320	293	600
20091121-07.fits	55 157.77206	0.2531	222	300	20100307-10.fits	55 263.64569	0.5980	296	600
20091121-08.fits	55 157.77950	0.2533	234	300	20100310-09.fits	55 266.63989	0.6643	221	600
20091130-02.fits	55 166.79663	0.4530	153	300	20100313-06.fits	55 269.63109	0.7306	215	600
20091130-03.fits	55 166.80047	0.4531	160	300	20100316-08.fits	55 272.61929	0.7968	328	600
20091209-08.fits	55 175.70075	0.6502	100	300	20100322-07.fits	55 278.62672	0.9298	265	600
20091209-09.fits	55 175.70490	0.6503	100	300	20100325-07.fits	55 281.60965	0.9959	276	900
20100109-09.fits	55 206.71990	0.3372	193	300	20100325-10.fits	55 281.69350	0.9977	287	900
20100109-10.fits	55 206.72635	0.3373	205	300	20100326-06.fits	55 282.57737	0.0173	333	900
20100111-12.fits	55 208.76993	0.3826	163	600	20100326-10.fits	55 282.68869	0.0198	314	900
20100112-09.fits	55 209.75303	0.4044	158	600	20100328-09.fits	55 284.60675	0.0623	400	600
20100114-07.fits	55 211.69796	0.4475	167	600	20100331-06.fits	55 287.57912	0.1281	274	600
20100116-07.fits	55 213.69359	0.4917	251	300					

Notes. The filename contains evening date of observation encoded as yyyymmdd. Barycentric Julian dates of mid-exposures are given. The S/N ratio was estimated from line-free continuum close to the Mg II 4481 line. Phases of mid-exposures were computed using the following ephemeris for the primary minimum: 2 447 832.0075 + 45.15023×E.

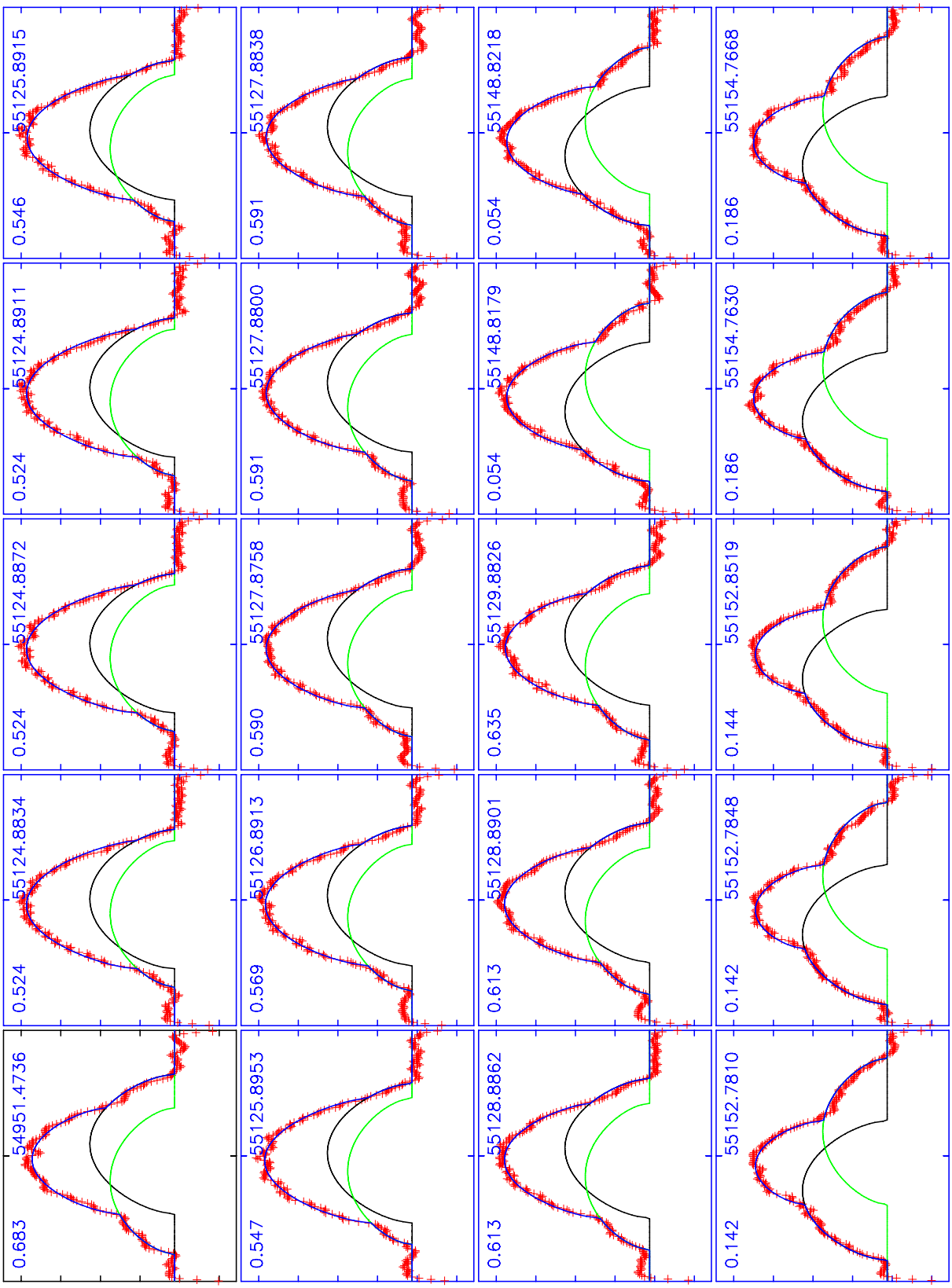

Fig. 5. Rotational profile fit to all broadening functions outside eclipses. The panels give the orbital phase and the heliocentric Julian date (with 2 400 000 subtracted). The profile of the primary component (Aa) is plotted in black, the profile of the secondary component (Ab) in green, and the combined profile in blue.

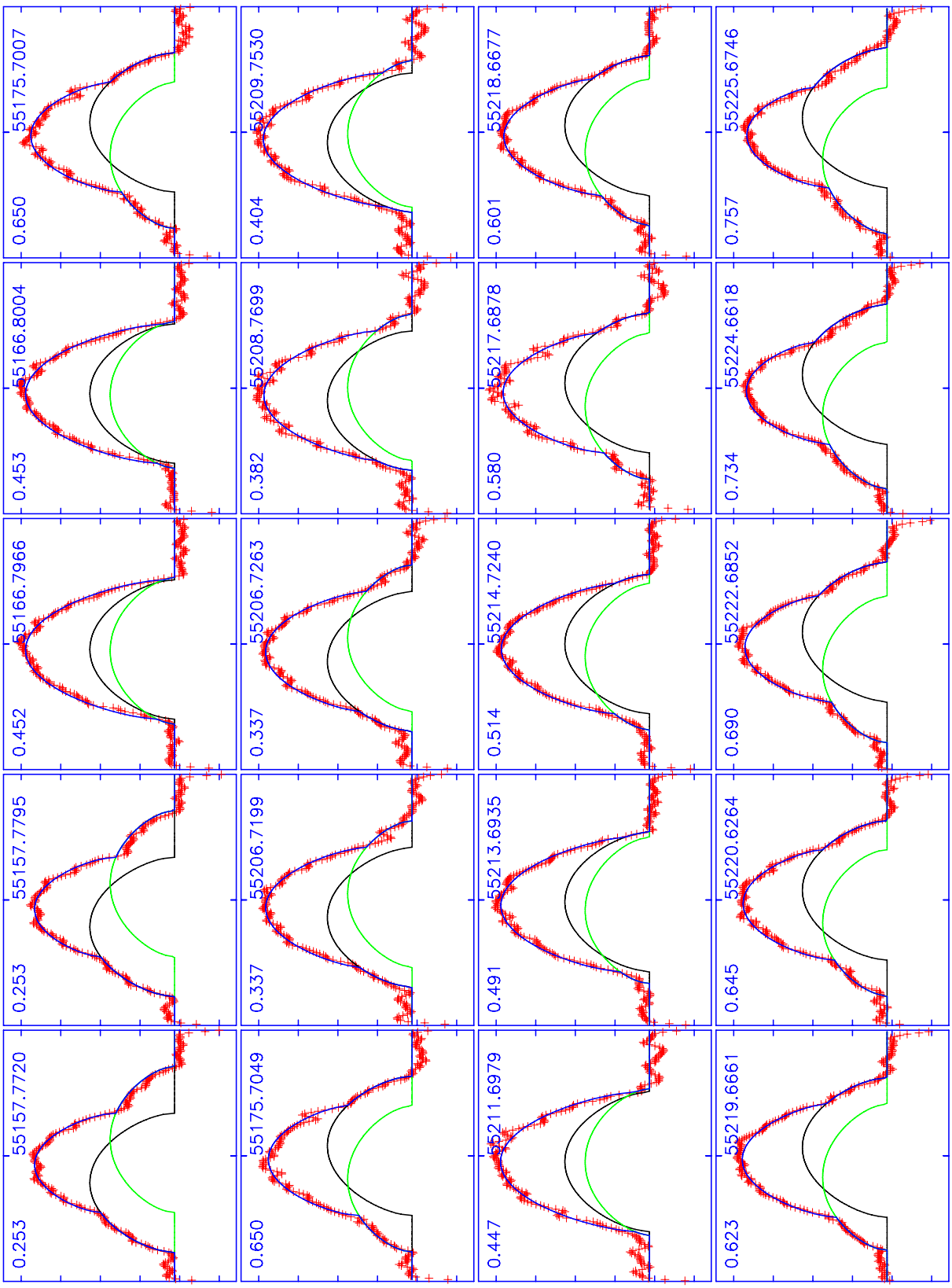

Fig. 5. continued.

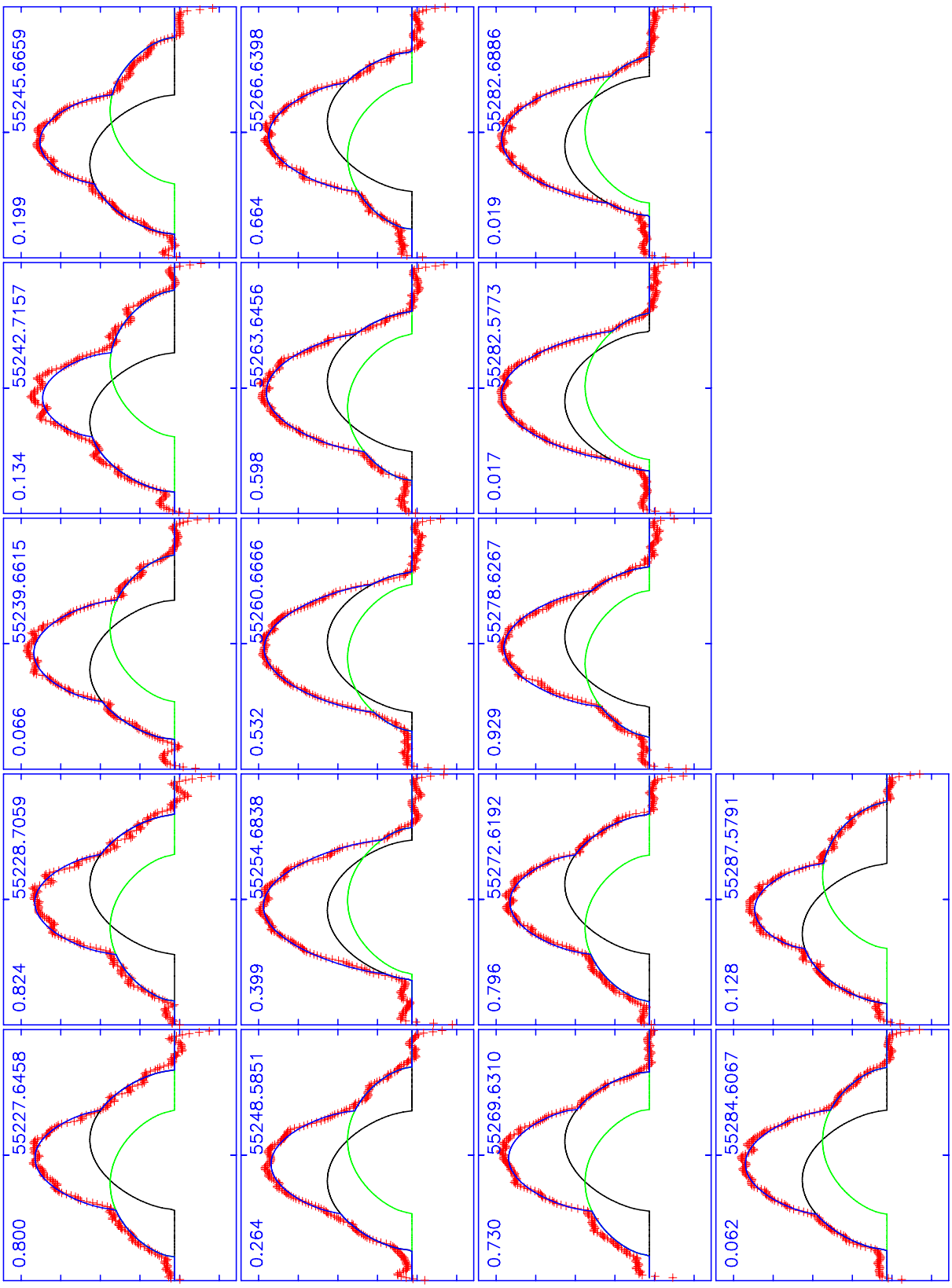

Fig. 5. continued.

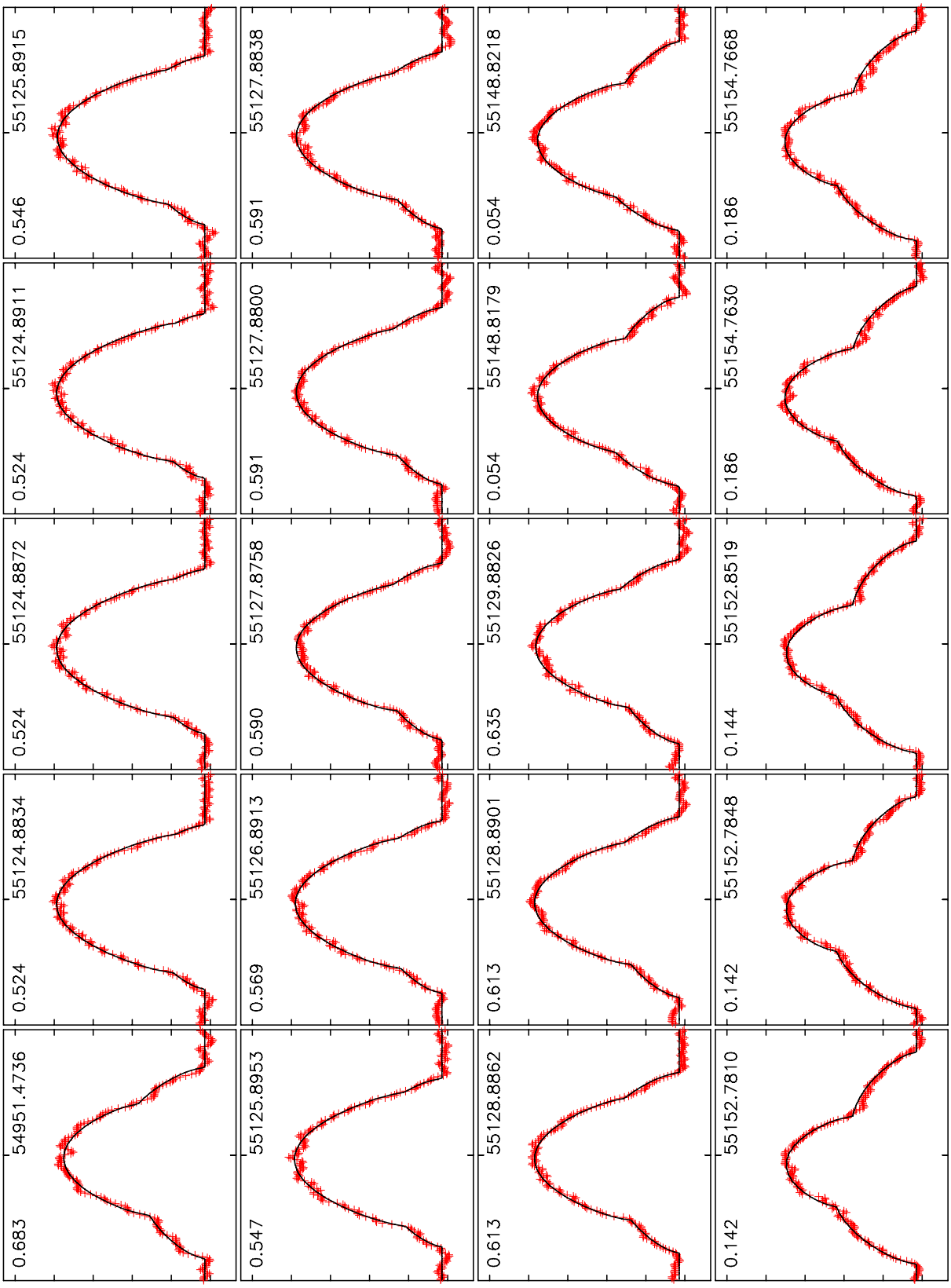

Fig. 6. The ROCHE-model fit to all broadening functions. The panels give the orbital phase and the heliocentric Julian date (with 2 400 000 subtracted).

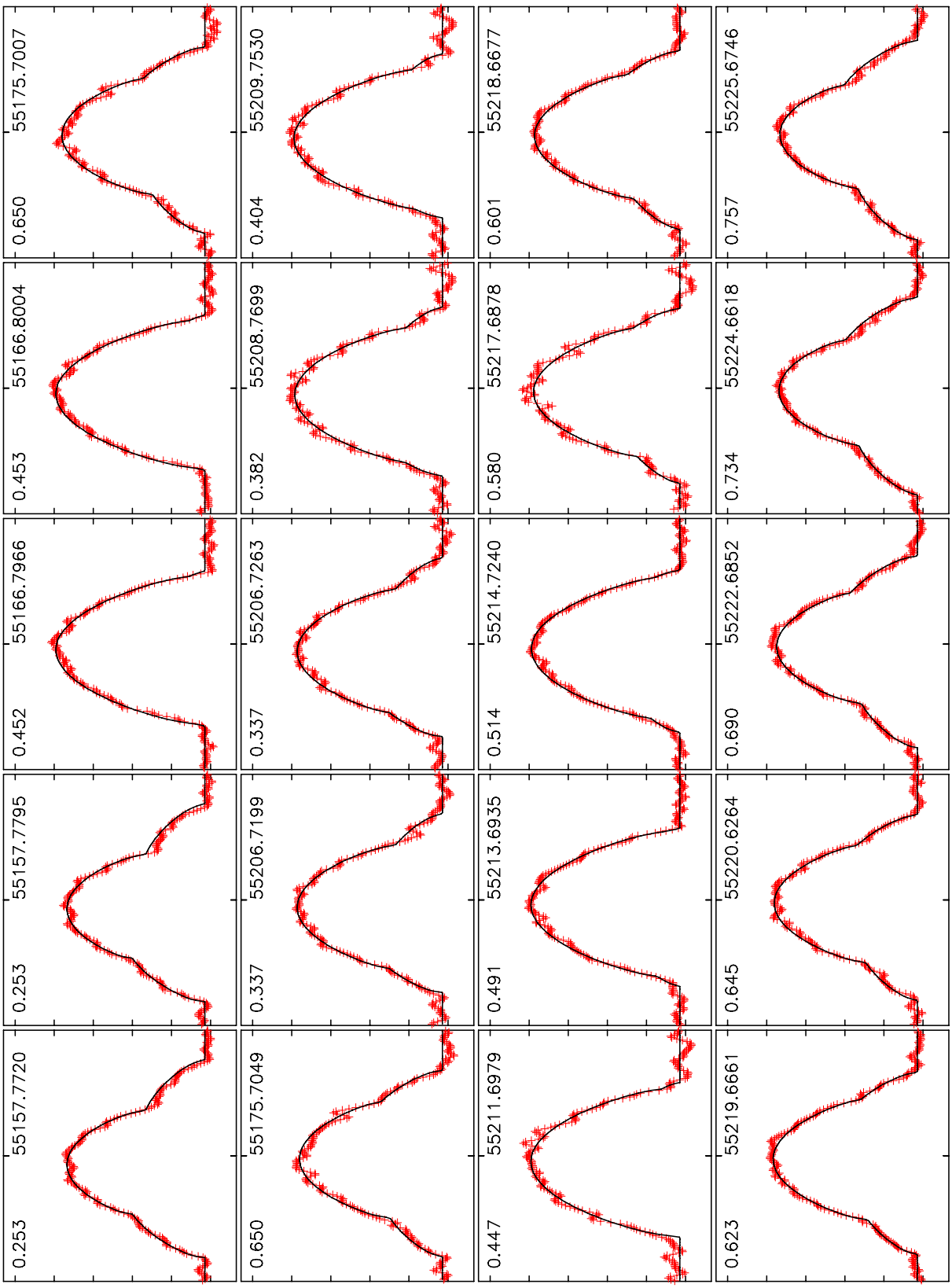

Fig. 6. continued.

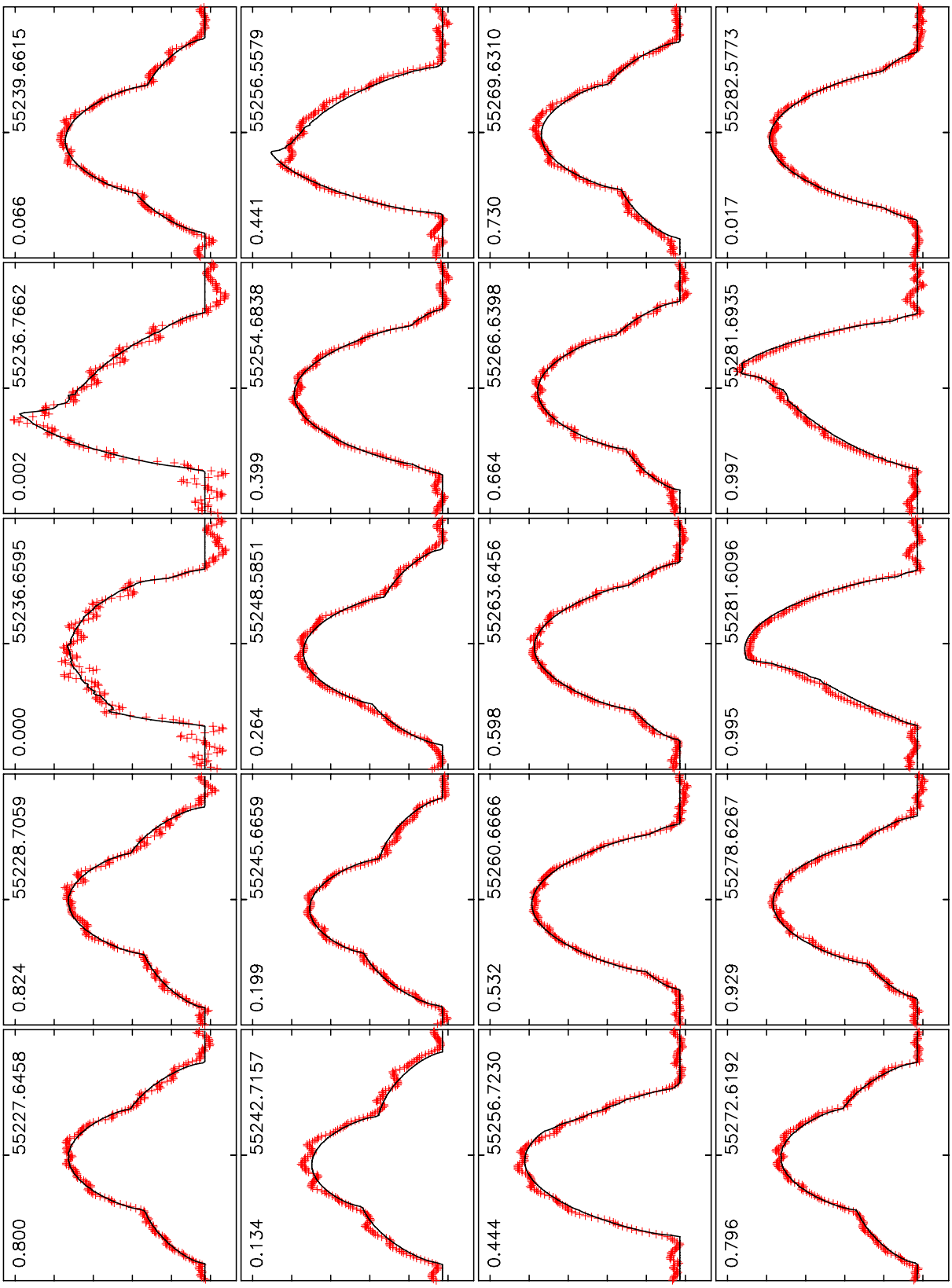

Fig. 6. continued.

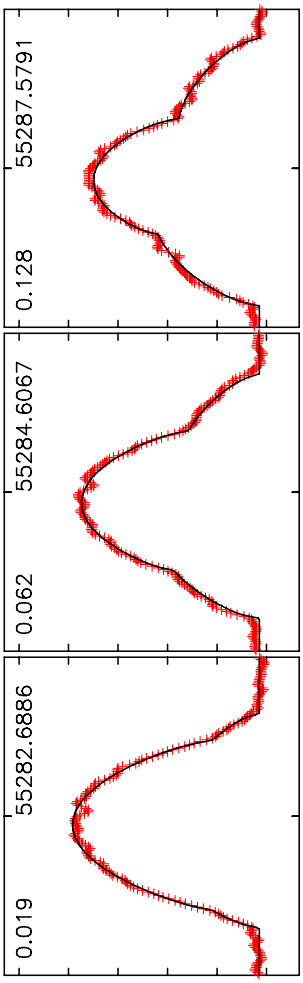

Fig. 6. continued.